
Evolving Generalizable Actor-Critic Algorithms

Juan Jose Garau-Luis^{1*†}, Yingjie Miao^{2†}, John D. Co-Reyes², Aaron Parisi²
Jie Tan², Esteban Real², Aleksandra Faust^{2†}
¹MIT, ²Google Brain

Abstract

Deploying Reinforcement Learning (RL) agents in the real world requires designing and tuning algorithms for problem-specific objectives such as performance, robustness, or stability. These objectives can frequently change, which will then necessitate further painstaking design and tuning. This paper presents MetaPG, an evolutionary method for designing new loss functions for actor-critic RL algorithms that optimize for different objectives. In particular, we focus on the objectives of final performance in training regime, policy robustness to unseen environment configurations, and training curve stability over random seeds. We initialize our algorithm population from Soft Actor-Critic (SAC) and optimize for these objectives over a set of continuous control tasks from the Real-World RL Benchmark Suite. We find that our method evolves algorithms that, using a single environment during evolution, improve upon SAC’s performance and generalizability by 3% and 17%, respectively, and reduce instability up to 65% in that same environment. Then, we scale up to more complex environments from the Brax physics simulator and replicate conditions that can be encountered in practical settings (such as different friction coefficients). MetaPG evolves algorithms that can obtain 9% better policy robustness within the same meta-training environment without loss of performance and robustness when doing cross-domain evaluations in other Brax environments. Lastly, we analyze the structure of the best algorithms in the population and interpret the specific elements that help the algorithm optimize for a certain objective, such as regularizing the critic loss.

1 Introduction

Many Reinforcement Learning (RL) practitioners working on real-world problems, besides aiming for strong performance, look for stable RL algorithms with good generalization that can be deployed with minimal human intervention. Deployed policies should perform well according to specific standards set in the training environment but at the same time should generalize to unseen scenarios with zero-shot learning. In addition, since policies are re-trained many times during the development process, RL algorithms should be stable, i.e., the training curve should be consistent across independent runs of the algorithm. Examples from domain-specific research (e.g., robotics [1], energy systems [2], fluid dynamics [3]) demonstrate the impact of this triad. When optimizing for these three objectives at the same time is not possible, domain experts make decisions over their preferences, which might change over time as the agent operates in the real world. Even for state-of-the-art RL algorithms, these challenges are considerably adverse in the context of real scenarios, either by themselves or in combination [4]. Prior work generally prioritizes optimizing for one objective over the rest, obviating the multi-preference perspective many real-world environments intrinsically require.

State-of-the-art RL algorithms, such as D4PG [5] or DMPO [6], fall short when policies face real-world challenges such as generalization to environment configurations not seen during training

*Work done while JGL interned at Google Brain

†Correspondence to: garau@mit.edu, yingjiemiao@google.com, and faust@google.com

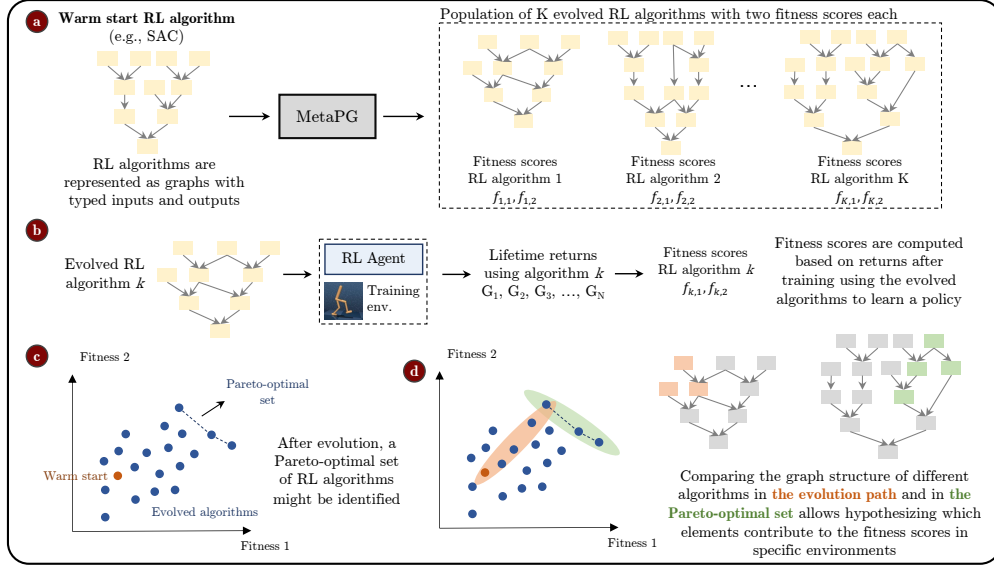


Figure 1: MetaPG overview, example with two fitness scores encoding two RL objectives. (a) The method starts by taking a warm-start RL algorithm with its loss function represented in the form of a directed acyclic graph. MetaPG consists of a meta evolution process that, after initializing algorithms to the warm-start, discovers a population of new algorithms. (b) Each evolved graph is evaluated by training an agent following the algorithm encoded by it, and then computing two fitness scores based on the training outcome. (c) After evolution, all RL algorithms can be represented in the fitness space and a Pareto-optimal set of algorithms can be identified. (d) Identifying which graph substructures change across the algorithms in the Pareto set allows to see which operations favor specific RL objectives. MetaPG can be scaled to more than two RL objectives.

(e.g., physical parameters of the environment are different) [4]. The impact is worse when multiple challenges are combined in one experiment [4]. While policy goodness is generally measured by average training return, domain-specific practitioners also value other objectives such as policy robustness to environmental perturbations and therefore, depending on the context, are willing to prioritize it and trade it for training performance [7]. This preference might shift due to multiple factors outside of the practitioner’s control [8]. In addition, stability is a well-known problem for RL [9]; and RL algorithms are seldom ranked according to this property. As current RL algorithm design tends to be different from this multi-preference setup, there is little knowledge on how to prioritize more than one goal at the same time and balance the tradeoffs.

Previous work propose multiple solutions to address individual goals [10, 11], the majority of them follow human-driven design processes. When we want to optimize for multiple objectives and our preferences vary, this poses two problems: 1) the costs of human-driven design might become prohibitively expensive when trying to optimize more than one RL objective or re-design is frequently required; and 2) it is unclear whether designing an all-purpose RL algorithm that works across domains is possible in these contexts. We argue multi-preference RL builds the case for automating algorithm design and speeding up the process of RL algorithm discovery. Automated Machine Learning or AutoML [12] has proven to be a successful tool for Supervised Learning problems [13–16], and it has been recently applied in the context of RL for automating loss function search [17–20].

This paper proposes MetaPG (see Figure 1), a method that evolves a population of continuous action actor-critic algorithms [21], identified by their loss functions³; loss functions are represented as directed acyclic graphs, using multiple fitness scores encoding independent RL objectives that are taken into account by means of the multi-objective ranking algorithm NSGA-II [22]. Compared to manual design, this strategy allows us to explore the algorithm space more efficiently by automating search operations. MetaPG finds algorithm improvement directions that jointly optimize the objectives

³In this work we use the term algorithm and loss function interchangeably

considered until it obtains a Pareto-optimal set of loss functions that maximizes fitness with respect to each objective, approximating the underlying tradeoff among them.

To evaluate MetaPG, we carry out multi-objective experiments using, first, the Real-World RL environment suite [4], which provides benchmarks for generalization under physical perturbations; and second, the Ant and Humanoid environments from the Brax physical simulator [23]. We warm-start the evolution with a graph-based representation of Soft Actor-Critic (SAC) [24], and demonstrate that our method is able to evolve a Pareto-optimal set of actor-critic algorithms that improve SAC’s performance and generalizability by 3% and 17%, respectively, and reduce instability up to 65%. We use a single environment class during evolution (e.g., Cartpole) and evaluate the improvements in that same class. Then, using the same warm-starting procedure in the Brax environments, we find algorithms that, after hyperparameter-tuning, outperform SAC by 12%, 9%, and 24% in performance, generalizability, and stability, respectively. Furthermore, we observe that algorithms evolved in Ant show minimal performance and generalizability loss when transferred to Humanoid and vice versa. Their metrics in the new environment are comparable to SAC’s after hyperparameter-tuning. Finally, since loss functions are represented as graphs, by comparing the structure of loss functions in different points of the fitness space, we can offer an interpretation of which substructures influence the observed fitnesses for the environments considered. For instance, we find MetaPG evolves loss functions that remove the entropy term in SAC to trade performance for generalizability.

In summary, this paper makes three main empirical contributions. The first contribution is a method that combines multi-objective evolution with a search language representing actor-critic algorithms as graphs, which can discover new loss functions over a set of different objectives. The second contribution consists of our encoding of stability, training performance, and policy generalization over environment perturbations as a specific set of objectives to optimize. The last contribution is a dataset⁴ of Pareto-optimal actor-critic loss functions which outperform baselines like SAC on multiple objectives. This dataset can hopefully be further analyzed to understand how algorithmic changes affect the tradeoff between these different objectives.

We believe this paper would be of interest to the broader RL community, as it highlights an important aspect of designing RL algorithms for practical applications: the balancing of different preferences over multiple objectives that together pose bottlenecks for deployment. Our findings can benefit AutoML research; as automating RL still remains a complex research problem, our work provides a new method aligned with practical goals and insights on interpretable loss function optimization. Lastly, this work also interests domain-specific practitioners; it provides a way of encoding their—possibly multiple—problem needs and picking the algorithm whose tradeoffs align better with the practical goals. The latter might not always be possible with current all-purpose RL algorithms.

2 Related Work

RL with multiple reward signals Certain environments intrinsically provide multiple reward signals in the form of different benefits and/or costs. Number of techniques handle those scenarios: reducing all reward signals into a single scalar [25], combining in the distribution space individual policies trained for each signal [26], training one policy per preference over rewards [27, 28], or meta learning to automate reward search [29, 30]. Our work does not focus on accounting for multiple reward signals. Instead, it focuses on RL algorithms that, in addition to optimizing for a cumulative reward, also optimize for the stability and generalization objectives, objectives desired in many real-world applications.

Optimizing for real-world RL objectives A large body of works identifies various application-specific RL objectives [4, 1, 31, 32]. For example, specific algorithms address individual objectives (e.g., Offline RL [33], safe RL [34], generalization [11]). However, multi-objective optimization for combinations of these objectives is seldom a goal in the literature, despite practitioners valuing combining them or establishing different sets of preferences. We frame our method as a multi-objective optimization of RL objectives (in our case performance, generalizability, and stability), in which relevant goals are simultaneously encoded.

Optimizing RL components Automated RL or AutoRL seeks to meta learn RL components [35], such as RL algorithms [17, 36, 18, 20], their hyperparameters [37–39], policy/neural network [40, 41],

⁴The dataset can be found at: <https://github.com/authors2022/dataset>

or the environment [42–46]. This work evolves RL algorithms and leaves other elements of the RL problem out of the scope. We focus on the RL algorithm given its interaction with all elements in a RL problem: states, actions, rewards, and the policy.

Evolutionary AutoML Neuro-evolution introduced evolutionary methods in the context of AutoML [47, 48], including neural network architecture search [49, 50, 15]. In the RL context evolution searched for policy gradients [51] and value iteration losses [17]. Our work is also related to the field of genetic programming, in which the goal is to discover computer code [52, 53, 17]. In this work we use a multi-objective evolutionary method to discover new RL algorithms, specifically actor-critic algorithms [21], represented as graphs that do not have meta parameters to be learned.

Learning RL algorithms Loss functions play a central role in RL algorithms and are traditionally designed by human experts. Recently, several lines of work propose to view RL loss functions as tunable objects that can be optimized automatically [35]. One popular approach is to use neural loss functions whose parameters are optimized via meta-gradient [36, 20, 18, 19]. An alternative is to use symbolic representations of loss functions and formulate the problem as optimizing over a combinatorial space. One example is [54], which represents extrinsic rewards as a graph and optimizes it by cleverly pruning a search space. Learning value-based RL loss functions was first proposed in [17], and was applied to solving discrete action problems. In contrast, MetaPG focuses on continuous control problems and searches for symbolic loss functions of actor-critic algorithms.

3 Methods

We represent actor-critic loss functions (policy loss and critic loss) as directed acyclic graphs and use an evolutionary algorithm to evolve a population of graphs, which are ranked based on their fitness scores. The population is seeded or warm-started with known algorithms such as SAC and undergoes mutations over time. Each graph’s fitnesses are measured by training from scratch an RL agent with the corresponding loss function and encode three objectives: performance, generalizability, and stability. We use the multi-objective evolutionary algorithm NSGA-II [22] to jointly optimize all objectives until growing a Pareto-optimal set of graphs. Algorithm 1 in Appendix B summarizes the process. Section 3.1 provides RL algorithm graph representation details. Then, the main logic of MetaPG is contained in the evaluation routine, which computes fitness scores (Section 3.2) and employs several techniques to speed up the evolution and evaluation processes (Section 3.3). See Appendix B for further implementation details.

3.1 RL algorithm representation

MetaPG encodes loss functions as graphs consisting of typed nodes sufficient to represent a wide class of actor-critic algorithms. Compared to the prior value-based RL evolutionary search [17], MetaPG search space greatly expands on it and adds types to manage the search complexity. As a representative example, Appendix D presents the encoding for SAC that we use in this paper. In our experiments we limit the number of nodes per graph to 60 and 80, which supposes searching over a space of approximately 10^{300} and 10^{400} graphs, respectively (see Appendix A). Nodes in the graph encode loss function inputs, operations, and loss function outputs. The inputs include elements from experience tuples, constants such as the discount factor γ , a policy network π , and multiple critic networks Q_i . Operation nodes support intermediate algorithm instructions such as basic arithmetic or array and neural network operations. Then, the outputs of the graphs correspond to the policy and critic losses. The gradient descent minimization process takes these outputs and computes their gradient with respect to the respective network parameters. In Appendix A we provide a full description of the search language and nodes considered. MetaPG’s search language supports both on-policy and off-policy algorithms; however, in this paper we focus on off-policy algorithms given their better sample efficiency.

3.2 Fitness scores

This work focuses on optimizing single-task performance, zero-shot generalizability, and stability across independent runs with different random seeds. To compute the fitness scores we rely on a set of environments \mathcal{E} , which comprises multiple instances of the same environment class, including a training instance $E_{train} \in \mathcal{E}$. For example, \mathcal{E} is the set of all RWRL Cartpole environments with

different pole lengths (0.1 meters to 3.0 meters in 0.1 intervals), and E_{train} corresponds to an instance with a specific pole length (1.0 meters). Using E_{train} to train a policy π , the performance score f_{perf} is the average evaluation return on the training environment configuration:

$$f_{perf} = \frac{1}{N_{eval}} \sum_{n=1}^{N_{eval}} G(\pi, E_{train}), \quad (1)$$

where G corresponds to the normalized episode return given a policy and an environment instance, and N_{eval} is the number of evaluation episodes. The generalizability score f_{gen} is in turn computed as the average evaluation return of the policy trained on E_{train} over the whole range of environment configurations. We emphasize that the policy is trained on a single environment configuration (for example 1.0 meter pole length) and then is evaluated in a zero-shot fashion to new unseen environment configurations:⁵

$$f_{gen} = \frac{1}{|\mathcal{E}|N_{eval}} \sum_{E \in \mathcal{E}} \sum_{n=1}^{N_{eval}} G(\pi, E) \quad (2)$$

Finally, stability entails getting consistent training curves across independent runs of the algorithm, mitigating the effect of stochastic elements. In that sense, stability is needed across objectives, as performance and generalizability should be consistent too. To that end, we leverage multiple random seeds; let f be a score (performance or generalizability), we measure f multiple times by running the RL training loop using N seeds. Then, we define *stability-adjusted* score as:

$$\tilde{f} = \mu(\{f_n\}_{n=1}^N) - \kappa \cdot \sigma(\{f_n\}_{n=1}^N) \quad (3)$$

where f_n denotes the score for seed n ; μ and σ are the mean and standard deviation across the N seeds, respectively; and κ is a penalization coefficient. The final fitness of a graph is the tuple $(\tilde{f}_{perf}, \tilde{f}_{gen})$.

3.3 Evolution details

Mutation The population is initialized with a provided RL algorithm as a warm-start; all individuals are copies of this algorithm’s graph at the beginning. Once the population is initialized, individuals undergo mutations that change the structure of their respective graphs. Specifically, mutations consist of either replacing one or more nodes in the graph or switching the connections for one edge. The specific number of nodes that are affected by mutation is randomly sampled for each different individual; see Appendix B for more details.

Operation consistency To prevent introducing corrupted child graphs into the population, MetaPG checks operation consistency, i.e., for each operation, it makes sure the shapes of the input tensors are valid and compatible, and computes the shape of the output tensor. These shapes and checks are propagated along the computation graph.

Hashing To avoid repeated evaluations, MetaPG hashes [53] all graphs in the population. Once the method produces a child graph and proves its consistency, it computes a hash value and, in case of cache hit, reuses the fitness score from the older individual in the population. In our case, we not only want to make sure that we do not evaluate the same graph twice, but also identify graphs that are different in form but identical in function. To that end, before hashing we prune all graphs so that only nodes that contribute to the output are taken into account. Then, we look at the gradients of the output losses with respect to the input parameters and use their concatenation as the hash value. In this process we use a fixed set of synthetic inputs.

Hurdle evaluations We carry out evaluations for different individuals in the population in parallel, while evaluating across seeds for one algorithm is done sequentially. To prevent spending too many resources on algorithms that are likely to yield bad policies, MetaPG uses a simple hurdle environment [17] and a number of hurdle seeds. We first evaluate the algorithm on the hurdle environment for each hurdle seed, and only proceed with more complex and computationally and expensive environments if the resulting policy performs above a certain threshold on the hurdle environment.

⁵More precisely, should be $E \in \mathcal{E}$ except E_{train} . In practice, we find this makes no significant difference in the metric because the number of test configurations is normally around 30.

4 Results

This section aims to answer the following questions: 1) Is MetaPG capable of evolving algorithms that improve upon the three objectives in different practical settings? 2) How well do discovered algorithms do in environments different from those used to evolve them? 3) Can we derive an explanation of what influences the scores of specific algorithms by looking at their graph structure?

We divide the experiments into meta training, meta validation, and meta testing phases. Each MetaPG run begins with the evolution process described in the previous section; this corresponds to the meta training phase, in which a specific set of seeds S_{train} is used. After this phase, we obtain the population of algorithms, each with a pair of meta training fitness scores. Since the evolution process is non-deterministic, we run each experiment multiple times without configuration changes and aggregate all resulting populations into one single bigger population. Then, to avoid selecting algorithms that overfit to the set of seeds S_{train} , we reevaluate all algorithms in the population with a different set of seeds S_{valid} ; this corresponds to the meta validation phase, which provides updated fitness scores for all algorithms. Finally, to assess the fitness of specific algorithms when deployed in different environments, we use a third set of seeds S_{test} that provides realistic fitness scores in the new environments; this corresponds to the meta testing phase. In our analyses of the results, we focus on the set of meta-validated algorithms and then meta-test some of them.

4.1 Training setup

Training environments We use as training environments: Cartpole and Walker from the RWRL Environment Suite [4], Gym Pendulum, and Ant and Humanoid from the Brax physics simulator [23]. We define different instances of these environments by varying the pole length in Cartpole, the thigh length in Walker, the pendulum length and mass in Pendulum, and, to mimic a practical setting, the mass, friction coefficient, and torque in Ant and Humanoid. See Appendix C for the specifics.

Meta training details The population and maximum graph size consist of 100 individuals and 80 nodes in the Brax environments, respectively, and 1,000 individuals and 60 nodes in the rest of the environments. All are initialized using SAC as a warm-start (see Appendix D). For RL algorithm evaluation, we use 10 different seeds S_{train} and fix the number of evaluation episodes N_{eval} to 20. In the case of Brax, since training takes longer, we use 4 different seeds but increase N_{eval} to 32. We meta-train using 100 TPU 1x1 v2 chips for 4 days in the case of Brax environments ($\sim 200K$ and $\sim 50K$ evaluated graphs in Ant and Humanoid, respectively), and using 1,000 CPUs for 10 days in the rest of environments ($\sim 100K$ evaluated graphs per experiment). In all cases we normalize the fitness scores to the range $[0, 1]$. We set $\kappa = 1$ in (3). Additional details are in Appendix B.

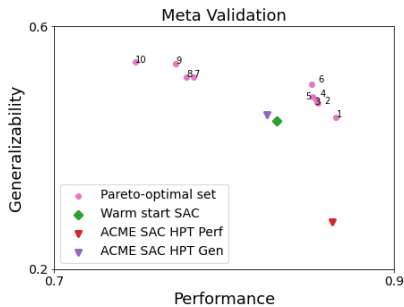
Meta validation details During meta validation, we use a set of 10 seeds S_{valid} , disjoint with respect to S_{train} . In the case of Brax environments, we use 4 meta validation seeds. Same applies during meta testing. In each case, we use a number of seeds that achieve a good balance between preventing overfitting and having affordable evaluation time. The value of N_{eval} during meta validation and meta testing matches the one used in meta training.

Hyperparameter tuning We use the same fixed hyperparameters during all meta training. Algorithms are also meta validated using the same hyperparameters. In the case of Brax environments, we do hyperparameter-tune the algorithms during meta validation; additional details can be found in Appendix F. We also hyperparameter-tune all baselines we compare our evolved algorithms against.

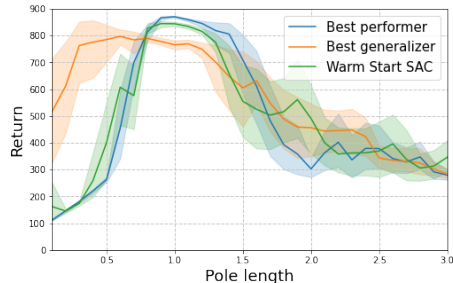
RL Training details The architecture of the policies corresponds to two-layer MLPs with 256 units each. Additional training details are presented in Appendix E.

4.2 Optimizing performance, generalizability, and stability in RWRL Environment Suite

We apply MetaPG to RWRL Cartpole and compare the evolved algorithms in the meta-validated Pareto-optimal set with the warm-start SAC and ACME SAC [55] (Figure 2a). When running ACME SAC we first do hyperparameter tuning and pick the two configurations that lead to the best performance and the best generalizability (ACME SAC HPT Perf and ACME SAC HPT Gen, respectively). In Table 1, we show numeric scores with standard errors. The results show that, by mutating the graphs, MetaPG discovers RL algorithms that improve upon the warm start’s and ACME SAC’s performance and generalizability in the same environment we used during evolution.



(a) Stability-adjusted fitness scores (computed using Equation 3) for algorithms in the Pareto-optimal set.



(b) Average return and standard deviation across seeds when evaluating trained policies in multiple RWRL Cartpole instances with different pole lengths (Training configuration is 1.0, see Appendix C).

Figure 2: Evolution results (meta validation across 10 different seeds) alongside the warm-start algorithm (SAC), and the hyperparameter-tuned ACME SAC when using the RWRL Cartpole environment for training. We show the Pareto-optimal set of algorithms that results after merging the 10 populations corresponding to the 10 repeats of the experiment. The best performer and best generalizer correspond to the algorithms with the highest stability-adjusted performance and generalizability scores, respectively, according to Equations 1, 2, and 3.

Table 1: Average performance and generalizability scores (Equations 1 and 2, respectively) \pm standard error of the mean for three algorithms in the Pareto-optimal set and SAC when using RWRL Cartpole as a training environment. We compute these metrics across 10 seeds.

RL Algorithm	Avg. Perf. score (f_{perf})	Avg. Gen. score (f_{gen})
Pareto point 1: Best performer	0.871 ± 0.003	0.475 ± 0.016
Pareto point 6	0.854 ± 0.002	0.531 ± 0.017
Pareto point 10: Best generalizer	0.770 ± 0.014	0.570 ± 0.019
warm-start SAC	0.845 ± 0.009	0.487 ± 0.027
ACME SAC HPT Perf	0.865 ± 0.001	0.372 ± 0.060
ACME SAC HPT Gen	0.845 ± 0.012	0.518 ± 0.040

Compared to the warm-start, the best performer achieves a 3% improvement in the performance score, the best generalizer achieves a 17% increase in the generalizability score, and the selected algorithm in the Pareto-optimal set (Pareto point 6) achieves a 1% and a 9% increase in both performance and generalizability, respectively. Then, in terms of the stability objective, evolved algorithms achieve between 33% and 65% reduction in the standard deviation of the results and therefore improve in that dimension as well. We repeat the same experiments in RWRL Walker and Gym Pendulum and observe that MetaPG also discovers a Pareto-optimal set of algorithms that outperform SAC in both environments. These results, as well as additional information on the stability of the algorithms, are in Appendix F.

Figure 2b compares how the best performer and the best generalizer behave in different instances of the environment in which we change the pole length (all instances form the environment set \mathcal{E} used during evolution). We follow the same procedure as described in [4]. The best performer achieves better return in the training configuration than the warm-start’s. The best generalizer in turn achieves a lower return but it trades it for higher returns in configurations outside of the training regime, being better at zero-shot generalization. The same behavior holds when using RWRL Walker and Gym Pendulum as training environments (see Appendix F).

4.3 Transferring evolved algorithms between Brax environments

Figure 3 shows the behaviour of evolved algorithms when meta-tested in Brax Ant, using an evaluation consisting of perturbations encountered in many practical settings (changes in friction coefficient, mass, and torque, see Appendix C). We first evolve algorithms independently in both Ant and Humanoid, then, for each case, select the algorithm with the best meta-training performance f_{perf} (in this case we focus on only one of the evolved algorithms since there is strong correlation between both metrics; the best performer and best generalizer are close, sometimes even encode the same

algorithm), then meta-validate it with different hyperparameter sets (see Appendix F), and select the hyperparameter set that leads to the best generalizability. We then fix the hyperparameters and re-evaluate using the meta-testing seeds. We compare algorithms evolved in Ant and Humanoid with hyperparameter-tuned SAC.

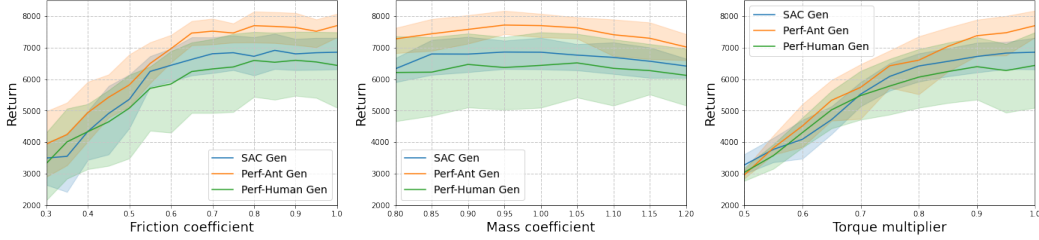


Figure 3: Average return and standard deviation across random seeds when evaluating evolved algorithms and SAC baseline in multiple Brax Ant instances with different friction coefficients, mass coefficients, and torque multipliers. We compare, after hyperparameter tuning, algorithms evolved in Brax Ant, Brax Humanoid (to assess cross-domain transfer), and the SAC baseline used as warm-start. In all cases 1.0 is used as training configuration.

These results highlight that, with proper hyperparameter tuning, an algorithm evolved by MetaPG in Brax Ant performs and generalizes better than a hyperparameter-tuned SAC baseline. Specifically, we observe a 12% improvement in performance and 9% improvement in generalizability. We also obtain a 24% reduction in instability. In addition, we observe that an algorithm initially evolved using Brax Humanoid and meta-validated in Ant transfers reasonably well to Ant during meta testing, achieving minimal loss of performance compared to hyperparameter-tuned SAC (6% less performance and 4% less generalizability compared to SAC). A similar result is obtained when Brax Humanoid environment serves as the meta testing environment (see Appendix F).

4.4 Analyzing the evolved RL algorithms

Next, we analyze evolved algorithms from our experiments on RWRL Cartpole. We pick the best meta-validated performer and generalizer, both evolved from the warm-start SAC (see Appendix D). The policy loss L_π and critic losses L_{Q_i} (one for each of the identical critic networks Q_i considered, see Appendix A) observed from the graph structure for the best performer are the following:

$$L_\pi^{perf} = \mathbb{E}_{(s_t, a_t, s_{t+1}) \sim \mathcal{D}} \left[\log(\min(\pi(\tilde{a}_{t+1} | s_{t+1}), \gamma)) - \min_i Q_i(s_t, \tilde{a}_t) \right] \quad (4)$$

$$L_{Q_i}^{perf} = \mathbb{E}_{(s_t, a_t, r_t, s_{t+1}) \sim \mathcal{D}} \left[(r_t + \gamma (Q_{target_i}(s_{t+1}, \tilde{a}_{t+1})) - Q_i(s_t, a_t))^2 \right] \quad (5)$$

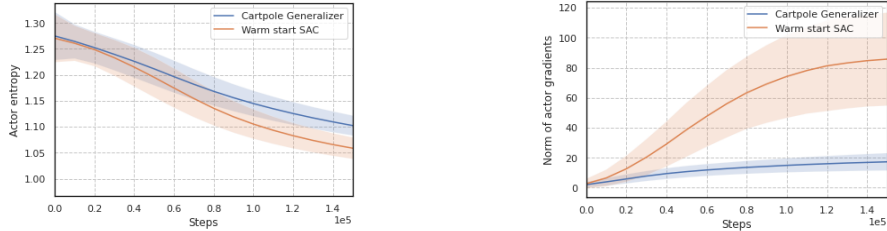
where $\tilde{a}_t \sim \pi(\cdot | s_t)$, $\tilde{a}_{t+1} \sim \pi(\cdot | s_{t+1})$, and \mathcal{D} is an experience dataset extracted from the replay buffer. Likewise, the loss equations for the best generalizer are:

$$L_\pi^{gen} = \mathbb{E}_{(s_t, a_t, s_{t+1}) \sim \mathcal{D}} \left[\log \pi(\tilde{a}_t | s_t) - \min_i Q_i(s_{t+1}, \tilde{a}_t) \right] \quad (6)$$

$$L_{Q_i}^{gen} = \mathbb{E}_{(s_t, a_t, r_t, s_{t+1}) \sim \mathcal{D}} \left[\text{atan} \left(\left(r_t + \gamma \left(\min_i Q_{target_i}(s_{t+1}, \tilde{a}_t) - \log \pi(\tilde{a}_t | s_t) \right) - Q_i(s_t, a_t) \right)^2 \right) \right] \quad (7)$$

While both algorithms resemble the warm-start SAC (see Appendix D), we observe that the best performer does not include the entropy term in the critic loss while the best generalizer does (i.e., they correspond to setting α to 0 and 1 in the original SAC algorithm [24], respectively). This aligns with the hypothesis that, since ignoring the entropy pushes the agent to exploit more and explore less, the policy of the best performer overfits better to the training configuration compared to SAC. In contrast, the best generalizer is able to explore more. Figure 4a validates the latter observation showing a higher entropy for the best generalizer’s actor compared to the warm-start’s.

The use of arctangent in the critic loss of the best generalizer is also noticeable as, supported by Figure 4b, we observe this operation serves as a way of clipping the loss, which makes gradients



(a) Average entropy of the policy during training for RWRL Cartpole. (b) Average gradient norm of the actor loss during training for RWRL Cartpole.

Figure 4: Analysis of the entropy and gradient norm of the actor when evaluating the best generalizer from RWRL Cartpole in comparison to the warm-start. We hypothesize this increase in entropy and decrease in gradient norm with respect to SAC contribute to achieve better generalizability.

smaller and thus prevents the policy’s parameters from changing too abruptly. In our experiments, we fix the number of training episodes as a compromise between achievable returns and evaluation runtimes. Clipping the loss has then an early-stopping effect compared to the baseline and results in a policy less overfitted, which benefits generalization. In Appendix F, we show both extended results that ignore the fix budget requirement and the equations for the best evolved algorithms in the remaining environments.

4.5 Discussion

Computational cost We acknowledge running MetaPG involves a non-negligible upfront computational cost. However, we believe this cost can be amortized by reusing the evolved algorithms; this is something that is aligned with the economy of scale AutoML approaches look for [56]. First, the cost is amortized by generating a Pareto-optimal set of loss functions from which practitioners can choose a specific point based on the desired performance vs. generalizability preference. A single-objective approach would require running MetaPG every time this preference changes. In addition, the achieved cross-domain generalization provides an additional perspective on amortizing the cost; we can reuse the algorithms across different domains and environments.

Improving evolution The Pareto-optimal set observed in Figure 2 combines 10 separate runs of evolution, since each individual run could converge to a different local optimum. We leave it to future work to improve the robustness of a single search experiment.

Potential value of interpolation between algorithms Our analyses have constantly focused on two extreme points from the Pareto-optimal sets (best performer and best generalizer). It is possible to interpolate between these two points to form an ensemble loss function. Such loss function may give additional flexibility for practitioners when designing an RL system by encoding complex design choices into an interpolation across objectives.

Cross-domain performance We have carried out cross-domain evaluation for Brax experiments and run additional experiments on the RWRL suite (see Appendix F). We have observed that, while evolved algorithms transfer reasonably well (especially best performers), sometimes they do not perform better than SAC in the new environments without hyperparameter tuning first, and that might not be enough in a small set of cases. This suggests that a direction of future work is to improve the transferrability of the evolved algorithms. At the same time, it poses an interesting research question of determining whether MetaPG is better suited to find “super algorithms” for specific environments or a new generation of all-purpose algorithms.

5 Conclusion

We presented MetaPG, a method that evolves actor-critic RL loss functions to optimize multiple RL objectives simultaneously and applied it to discovering algorithms that perform well, achieve zero-shot generalization across different environment configurations, and are stable; a triad of objectives with real-world implications. The experiments in RWRL Cartpole, RWRL Walker, and Gym Pendulum demonstrated that MetaPG discovered algorithms that, when using one environment

during evolution and then meta-validating in that same environment, outperform SAC, achieving a 3% and 17% improvement in performance and generalizability, respectively, and a reduction of 33% to 65% in instability. Experiments on Brax Ant and Brax Humanoid proved evolution is successful in more complex environments, achieving a 12% and 9% increase in performance and generalizability, respectively. We also observed that, when transferring evolved algorithms to environments different from those used during evolution, the loss of performance and generalizability in the new environment is minimal and is comparable to SAC. Finally, we have analyzed the evolved loss functions and linked specific elements in their structure to fitness results, such as the removal of the entropy term to benefit performance.

Contributions and Acknowledgments

JGL and AF conceived the project. AF assembled the team. JGL initiated research ideas, ran experiments and analysis. ER, AF, JT advised on evolutionary algorithms, reinforcement learning, and real-world applications, respectively. ER built the evolutionary infrastructure, with contributions from YM and AP. JGL developed the search space, with contributions from YM, JD, AP, and JT. JGL wrote the paper.

The authors want to thank Ramki Gummedi for helpful discussions, Hicham El Zein, Stephen Jonany, and Xinyu Feng for code contributions, and Izzeddin Gur for useful feedback.

References

- [1] Julian Ibarz, Jie Tan, Chelsea Finn, Mrinal Kalakrishnan, Peter Pastor, and Sergey Levine. How to train your robot with deep reinforcement learning: lessons we have learned. *The International Journal of Robotics Research*, 40(4-5):698–721, 2021.
- [2] A.T.D. Perera and Parameswaran Kamalaruban. Applications of reinforcement learning in energy systems. *Renewable and Sustainable Energy Reviews*, 137:110618, 2021.
- [3] Paul Garnier, Jonathan Viquerat, Jean Rabault, Aurélien Larcher, Alexander Kuhnle, and Elie Hachem. A review on deep reinforcement learning for fluid mechanics. *Computers & Fluids*, 225:104973, 2021.
- [4] Gabriel Dulac-Arnold, Nir Levine, Daniel J Mankowitz, Jerry Li, Cosmin Paduraru, Sven Gowal, and Todd Hester. Challenges of real-world reinforcement learning: definitions, benchmarks and analysis. *Machine Learning*, pages 1–50, 2021.
- [5] Gabriel Barth-Maron, Matthew W. Hoffman, David Budden, Will Dabney, Dan Horgan, Dhruva TB, Alistair Muldal, Nicolas Heess, and Timothy Lillicrap. Distributed distributional deterministic policy gradients, 2018.
- [6] Abbas Abdolmaleki, Jost Tobias Springenberg, Yuval Tassa, Remi Munos, Nicolas Heess, and Martin Riedmiller. Maximum a posteriori policy optimisation, 2018.
- [7] Hamed Rahimian and Sanjay Mehrotra. Distributionally robust optimization: A review, 2019.
- [8] Aleksandra Faust, Hao-Tien Lewis Chiang, and Lydia Tapia. Pearl: Preference appraisal reinforcement learning for motion planning. 2018.
- [9] Peter Henderson, Riashat Islam, Philip Bachman, Joelle Pineau, Doina Precup, and David Meger. Deep reinforcement learning that matters. In *Proceedings of the AAAI conference on artificial intelligence*, volume 32, 2018.
- [10] Esther Derman, Daniel J. Mankowitz, Timothy A. Mann, and Shie Mannor. Soft-robust actor-critic policy-gradient, 2018.
- [11] Robert Kirk, Amy Zhang, Edward Grefenstette, and Tim Rocktäschel. A survey of generalisation in deep reinforcement learning, 2022.
- [12] Frank Hutter, Lars Kotthoff, and Joaquin Vanschoren. *Automated machine learning: methods, systems, challenges*. Springer Nature, 2019.

- [13] Oriol Vinyals, Charles Blundell, Timothy Lillicrap, Daan Wierstra, et al. Matching networks for one shot learning. *Advances in neural information processing systems*, 29, 2016.
- [14] Barret Zoph, Vijay Vasudevan, Jonathon Shlens, and Quoc V Le. Learning transferable architectures for scalable image recognition. In *Proceedings of the IEEE conference on computer vision and pattern recognition*, pages 8697–8710, 2018.
- [15] Esteban Real, Alok Aggarwal, Yanping Huang, and Quoc V Le. Regularized evolution for image classifier architecture search. In *Proceedings of the aaai conference on artificial intelligence*, volume 33, pages 4780–4789, 2019.
- [16] Chelsea Finn, Pieter Abbeel, and Sergey Levine. Model-agnostic meta-learning for fast adaptation of deep networks. In *International conference on machine learning*, pages 1126–1135. PMLR, 2017.
- [17] John D Co-Reyes, Yingjie Miao, Daiyi Peng, Esteban Real, Sergey Levine, Quoc V Le, Honglak Lee, and Aleksandra Faust. Evolving reinforcement learning algorithms. In *International Conference on Learning Representations*, 2021.
- [18] Junhyuk Oh, Matteo Hessel, Wojciech M Czarnecki, Zhongwen Xu, Hado P van Hasselt, Satinder Singh, and David Silver. Discovering reinforcement learning algorithms. *Advances in Neural Information Processing Systems*, 33:1060–1070, 2020.
- [19] Zhongwen Xu, Hado P van Hasselt, Matteo Hessel, Junhyuk Oh, Satinder Singh, and David Silver. Meta-gradient reinforcement learning with an objective discovered online. *Advances in Neural Information Processing Systems*, 33:15254–15264, 2020.
- [20] Sarah Bechtle, Artem Molchanov, Yevgen Chebotar, Edward Grefenstette, Ludovic Righetti, Gaurav Sukhatme, and Franziska Meier. Meta Learning via Learned Loss. In *2020 25th International Conference on Pattern Recognition (ICPR)*, pages 4161–4168. IEEE, jan 2021.
- [21] Richard S Sutton and Andrew G Barto. *Reinforcement learning: An introduction*. MIT press, 2018.
- [22] Kalyanmoy Deb, Amrit Pratap, Sameer Agarwal, and TAMT Meyarivan. A fast and elitist multiobjective genetic algorithm: Nsga-ii. *IEEE transactions on evolutionary computation*, 6(2):182–197, 2002.
- [23] C. Daniel Freeman, Erik Frey, Anton Raichuk, Sertan Girgin, Igor Mordatch, and Olivier Bachem. Brax - a differentiable physics engine for large scale rigid body simulation, 2021.
- [24] Tuomas Haarnoja, Aurick Zhou, Pieter Abbeel, and Sergey Levine. Soft actor-critic: Off-policy maximum entropy deep reinforcement learning with a stochastic actor. In *International conference on machine learning*, pages 1861–1870. PMLR, 2018.
- [25] Mingxing Tan, Bo Chen, Ruoming Pang, Vijay Vasudevan, Mark Sandler, Andrew Howard, and Quoc V Le. Mnasnet: Platform-aware neural architecture search for mobile. In *Proceedings of the IEEE/CVF Conference on Computer Vision and Pattern Recognition*, pages 2820–2828, 2019.
- [26] Abbas Abdolmaleki, Sandy Huang, Leonard Hasenclever, Michael Neunert, Francis Song, Martina Zambelli, Murilo Martins, Nicolas Heess, Raia Hadsell, and Martin Riedmiller. A distributional view on multi-objective policy optimization. In *International Conference on Machine Learning*, pages 11–22. PMLR, 2020.
- [27] Jie Xu, Yunsheng Tian, Pingchuan Ma, Daniela Rus, Shinjiro Sueda, and Wojciech Matusik. Prediction-Guided Multi-Objective Reinforcement Learning for Continuous Robot Control. In *Proceedings of the 37th International Conference on Machine Learning*, 2020.
- [28] Runzhe Yang, Xingyuan Sun, and Karthik Narasimhan. A generalized algorithm for multi-objective reinforcement learning and policy adaptation. *Advances in Neural Information Processing Systems*, 32, 2019.

- [29] Xi Chen, Ali Ghadirzadeh, Marten Bjorkman, and Patric Jensfelt. Meta-Learning for Multi-objective Reinforcement Learning. In *2019 IEEE/RSJ International Conference on Intelligent Robots and Systems (IROS)*, pages 977–983. IEEE, nov 2019.
- [30] Aleksandra Faust, Anthony Francis, and Dar Mehta. Evolving Rewards to Automate Reinforcement Learning. may 2019.
- [31] Henry Zhu, Justin Yu, Abhishek Gupta, Dhruv Shah, Kristian Hartikainen, Avi Singh, Vikash Kumar, and Sergey Levine. The ingredients of real world robotic reinforcement learning. In *International Conference on Learning Representations*, 2020.
- [32] Juan Jose Garau-Luis, Edward Crawley, and Bruce Cameron. Evaluating the progress of deep reinforcement learning in the real world: aligning domain-agnostic and domain-specific research, 2021.
- [33] Sergey Levine, Aviral Kumar, George Tucker, and Justin Fu. Offline reinforcement learning: Tutorial, review, and perspectives on open problems. 2020.
- [34] Lukas Brunke, Melissa Greeff, Adam W Hall, Zhaocong Yuan, Siqi Zhou, Jacopo Panerati, and Angela P Schoellig. Safe learning in robotics: From learning-based control to safe reinforcement learning. *Annual Review of Control, Robotics, and Autonomous Systems*, 5, 2021.
- [35] Jack Parker-Holder, Raghu Rajan, Xingyou Song, André Biedenkapp, Yingjie Miao, Theresa Eimer, Baohe Zhang, Vu Nguyen, Roberto Calandra, Aleksandra Faust, Frank Hutter, and Marius Lindauer. Automated Reinforcement Learning (AutoRL): A Survey and Open Problems. 2022.
- [36] Louis Kirsch, Sjoerd van Steenkiste, and Juergen Schmidhuber. Improving generalization in meta reinforcement learning using learned objectives. In *International Conference on Learning Representations*, 2020.
- [37] Baohe Zhang, Raghu Rajan, Luis Pineda, Nathan Lambert, André Biedenkapp, Kurtland Chua, Frank Hutter, and Roberto Calandra. On the importance of hyperparameter optimization for model-based reinforcement learning. In Arindam Banerjee and Kenji Fukumizu, editors, *Proceedings of The 24th International Conference on Artificial Intelligence and Statistics*, volume 130 of *Proceedings of Machine Learning Research*, pages 4015–4023. PMLR, 13–15 Apr 2021.
- [38] Lars Hertel, Pierre Baldi, and Daniel L. Gillen. Quantity vs. quality: On hyperparameter optimization for deep reinforcement learning, 2020.
- [39] Zhongwen Xu, Hado P van Hasselt, and David Silver. Meta-gradient reinforcement learning. In S. Bengio, H. Wallach, H. Larochelle, K. Grauman, N. Cesa-Bianchi, and R. Garnett, editors, *Advances in Neural Information Processing Systems*, volume 31. Curran Associates, Inc., 2018.
- [40] Adam Gaier and David Ha. Weight agnostic neural networks. In H. Wallach, H. Larochelle, A. Beygelzimer, F. d’Alché Buc, E. Fox, and R. Garnett, editors, *Advances in Neural Information Processing Systems*, volume 32. Curran Associates, Inc., 2019.
- [41] Yingjie Miao, Xingyou Song, Daiyi Peng, Summer Yue, John D Co-Reyes, Eugene Brevdo, and Aleksandra Faust. RL-darts: differentiable architecture search for reinforcement learning. 2021.
- [42] Fabio Ferreira, Thomas Nierhoff, and Frank Hutter. Learning synthetic environments for reinforcement learning with evolution strategies, 2021.
- [43] Izzeddin Gur, Natasha Jaques, Yingjie Miao, Jongwook Choi, Manoj Tiwari, Honglak Lee, and Aleksandra Faust. Environment generation for zero-shot compositional reinforcement learning. In Marc’Aurelio Ranzato, Alina Beygelzimer, Yann N. Dauphin, Percy Liang, and Jennifer Wortman Vaughan, editors, *Advances in Neural Information Processing Systems 34: Annual Conference on Neural Information Processing Systems 2021, NeurIPS 2021, December 6-14, 2021, virtual*, pages 4157–4169, 2021.

- [44] Michael Dennis, Natasha Jaques, Eugene Vinitzky, Alexandre M. Bayen, Stuart Russell, Andrew Critch, and Sergey Levine. Emergent complexity and zero-shot transfer via unsupervised environment design. In Hugo Larochelle, Marc’Aurelio Ranzato, Raia Hadsell, Maria-Florina Balcan, and Hsuan-Tien Lin, editors, *Advances in Neural Information Processing Systems 33: Annual Conference on Neural Information Processing Systems 2020, NeurIPS 2020, December 6-12, 2020, virtual*, 2020.
- [45] Carlos Florensa, David Held, Xinyang Geng, and Pieter Abbeel. Automatic goal generation for reinforcement learning agents. In Jennifer Dy and Andreas Krause, editors, *Proceedings of the 35th International Conference on Machine Learning*, volume 80 of *Proceedings of Machine Learning Research*, pages 1515–1528. PMLR, 10–15 Jul 2018.
- [46] Vanessa Volz, Jacob Schrum, Jialin Liu, Simon M Lucas, Adam Smith, and Sebastian Risi. Evolving mario levels in the latent space of a deep convolutional generative adversarial network. In *Proceedings of the genetic and evolutionary computation conference*, pages 221–228, 2018.
- [47] Geoffrey F Miller, Peter M Todd, and Shailesh U Hegde. Designing neural networks using genetic algorithms. In *ICGA*, volume 89, pages 379–384, 1989.
- [48] Kenneth O Stanley and Risto Miikkulainen. Evolving neural networks through augmenting topologies. *Evolutionary computation*, 10(2):99–127, 2002.
- [49] Kenneth O Stanley, David B D’Ambrosio, and Jason Gauci. A hypercube-based encoding for evolving large-scale neural networks. *Artificial life*, 15(2):185–212, 2009.
- [50] Rafal Jozefowicz, Wojciech Zaremba, and Ilya Sutskever. An empirical exploration of recurrent network architectures. In *International conference on machine learning*, pages 2342–2350. PMLR, 2015.
- [51] Rein Houthoofd, Yuhua Chen, Phillip Isola, Bradly Stadie, Filip Wolski, OpenAI Jonathan Ho, and Pieter Abbeel. Evolved policy gradients. In *Advances in Neural Information Processing Systems*, pages 5400–5409, 2018.
- [52] John R Koza. Genetic programming as a means for programming computers by natural selection. *Statistics and computing*, 4(2):87–112, 1994.
- [53] Esteban Real, Chen Liang, David So, and Quoc Le. Automl-zero: Evolving machine learning algorithms from scratch. In *International Conference on Machine Learning*, pages 8007–8019. PMLR, 2020.
- [54] Ferran Alet, Martin F Schneider, Tomas Lozano-Perez, and Leslie Pack Kaelbling. Meta-learning curiosity algorithms. In *International Conference on Learning Representations*, 2019.
- [55] Matt Hoffman, Bobak Shahriari, John Aslanides, Gabriel Barth-Maron, Feryal Behbahani, Tamara Norman, Abbas Abdolmaleki, Albin Cassirer, Fan Yang, Kate Baumli, Sarah Henderson, Alex Novikov, Sergio Gómez Colmenarejo, Serkan Cabi, Caglar Gulcehre, Tom Le Paine, Andrew Cowie, Ziyu Wang, Bilal Piot, and Nando de Freitas. Acme: A research framework for distributed reinforcement learning, 2020.
- [56] David Patterson, Joseph Gonzalez, Quoc Le, Chen Liang, Lluís-Miquel Munguia, Daniel Rothchild, David So, Maud Texier, and Jeff Dean. Carbon emissions and large neural network training. 2021.
- [57] John Schulman, Filip Wolski, Prafulla Dhariwal, Alec Radford, and Oleg Klimov. Proximal policy optimization algorithms. 2017.

A Search space details

In this section we present the details of the search space; we divide the nodes into input, output, and operation nodes. Output nodes correspond to losses computed by the algorithm, whose gradient with respect to the algorithm inputs is then computed in a training loop. In this paper we do steepest gradient descent to update network parameters; given the search space complexity, we leave incorporating other gradient descent strategies into the search space out of its scope. However, other strategies such as natural gradient or conjugate gradient could be incorporated, as they do gradient transformations and are agnostic to loss functions.

In the training process, agents then learn the policy by means of experience tuples coming from a replay buffer. MetaPG admits both continuous and discrete action spaces; specific nodes in the graphs—e.g., the networks—are adapted to work with the corresponding space.

During the evolution process, we fix a maximum number of nodes, which consists of the aforementioned input and output nodes, and several operation nodes. The majority of operation nodes treat input elements as tensors with variable shapes in order to maximize graph flexibility. Each node possesses a certain number of input and output edges, which are determined by the specific operation this node carries out. For example, a node that takes in two tensors and multiplies them element-wise has two input edges and a single output edge.

A.1 List of nodes

A complete list of the nodes considered follows:

Input nodes We only encode canonical RL elements as inputs:

- Policy network π
- Two critic networks, Q_1 and Q_2 , and two target critic networks, Q_{targ_1} and Q_{targ_2}
- Batch of states s_t and next states s_{t+1}
- Batch of actions a_t
- Batch of rewards r_t
- Discount factor γ

Output nodes The output of these nodes is used as loss function to compute gradient descent on:

- Policy loss L_π
- Critic loss L_{Q_i}

Operation nodes These nodes operate generally on tensors and can broadcast operations when input sizes do not match:

- Addition: add two, three, or four tensors
- Multiplication: compute element-wise product of two or three tensors
- Subtract two tensors
- Divide two tensors and add constant ϵ to the denominator
- Neural network operations: Action distribution from state, stopping gradient computation
- Operations with action distributions: Sample, Log-probability
- Mean, sum, and standard deviation over last axis of array or over entire array
- Cumulative sum, cumulative sum with discount
- Squared difference
- Multiply by a constant: -1, 0.1, 0.01, 0.5, 2.0
- Minimum and maximum over last axis of a tensor
- Minimum and maximum element-wise between two tensors
- Other general operations: clamp, absolute value, square, logarithm, exponential
- Trigonometry functions

A.2 Size of the search space

To get an upper bound of the size of the search space in terms of the number of possible graphs (not all of them valid), we consider the $(k+1)$ -th node in the graph of size K nodes. This node can correspond to one of the N different operation nodes. Assuming that this node has two inputs, there are $\binom{k}{2}$ possibilities of connecting to previous nodes in the graph. Therefore, we have a total of $\frac{1}{2}Nk(k-1)$ possible combinations for the $(k+1)$ -th node. Then, an upper bound of the total number of possible graphs is

$$\left(\frac{NK(K-1)}{2}\right)^K \quad (8)$$

With $N = 33$ and $K = 60$ we obtain approximately 10^{286} graphs. This number increases to 10^{401} if $K = 80$ instead.

B Additional implementation details

Multi-objective evolution Algorithm 1 details the evolution process for MetaPG, in which `Offspring` and `RankAndSelect` are NSGA-II subroutines [22]. We do 10 independent repeats of MetaPG when evolving on RWRL Cartpole, RWRL Walker, and Gym Pendulum; 5 repeats when evolving on Brax Ant; and 3 repeats for Brax Humanoid.

Algorithm 1 MetaPG Overview

Input: Training environments \mathcal{E}

Initialize: Initialize population P_0 of loss function graphs (random initialization or bootstrap with an algorithm such as SAC).

```

1: for  $L$  in  $P_0$  do  $L.score \leftarrow \text{Eval}(L, \mathcal{E})$ 
2: end for
3:  $Q_0 \leftarrow \text{Offspring}(P_0)$  ▷ NSGA-II
4: for  $L$  in  $Q_0$  do  $L.score \leftarrow \text{Eval}(L, \mathcal{E})$ 
5: end for
6: for  $t = 1$  to  $G$  do
7:    $R \leftarrow P_{t-1} \cup Q_{t-1}$ 
8:    $P_t \leftarrow \text{RankAndSelect}(R)$  ▷ NSGA-II
9:    $Q_t \leftarrow \text{Offspring}(P_t)$  ▷ NSGA-II
10:  for  $L$  in  $Q_t$  do  $L.score \leftarrow \text{Eval}(L, \mathcal{E})$ 
11:  end for
12: end for
13: Output: Pareto-front of all loss function graphs.

```

Warm-starting Algorithms are initialized using the warm-start SAC graph (see Appendix D), which consists of 33 nodes. Additional operation nodes are added to each individual until reaching the maximum amount of 60 nodes.

Mutation During mutation, there is a 50% chance an individual undergoes node mutation and a 50% chance it undergoes edge mutation. During node mutation, there is a 50% chance of replacing one node, a 25% chance of replacing 2 nodes, a 12.5% chance of replacing 4 nodes, and a 6.25% chance of replacing 8 and 16 nodes, respectively. During edge mutation, only one edge in the graph is replaced.

Hashing In the hashing process we use a fixed set of synthetic inputs with a batch size of 16.

Encoding multiple objectives MetaPG keeps the population to a fixed size during evolution. To decide which individuals should be removed in the process, the method makes use of different fitness scores that encode each of the RL objectives considered. These scores are not combined but treated separately in a multi-objective fashion. This means that, after evaluating a graph i , it will have fitness

scores $\{f_{i,1}, f_{i,2}, \dots, f_{i,F}\}$, where F is the number of objectives considered. Then, when comparing two graphs i and j , we say i has higher fitness than j iff $f_{i,k} \geq f_{j,k}, \forall k$, with at least one fitness score k' such that $f_{i,k'} > f_{j,k'}$. In this case we also say graph i Pareto-dominates graph j . If neither i Pareto-dominates j nor vice versa, we say both graphs are Pareto-optimal.

The process of removing individuals from the population follows the NSGA-II algorithm [22] which, assuming a maximum population size of P_{max} individuals:

1. From a set of P individuals, with $|P| > P_{max}$, it computes the set P_{opt} of Pareto-optimal fittest graphs. None of the graphs in P_{opt} is Pareto-dominated by any other graph in the population and, if a graph i in P is Pareto-dominated by at least one other graph, then i does not belong to the Pareto-optimal set.
2. If $|P_{opt}| \geq P_{max}$, the graphs are ranked based on their crowding distance in the fitness space. This favors individuals that are further apart from other individuals in the fitness space. The fittest P_{max} individuals of the Pareto-optimal set P_{opt} are kept in the population.
3. Otherwise, if $|P_{opt}| < P_{max}$, the set P_{opt} is kept in the population and the process is repeated taking $P \leftarrow P \setminus P_{opt}$ and $P_{max} \leftarrow P_{max} - |P_{opt}|$.

Computational cost vs. performance Figure 5 shows the evolution of the best fitness in the population with respect to the total number of graphs evolved in the case of RWRL Cartpole; 10 independent runs of the same experiment are shown. It can be observed that the largest jumps in stability-adjusted performance and generalizability occur in the first 10% and 25% of individual evaluations, respectively. The stochastic nature of an individual experiment can lead to different outcomes with shorter or longer distances between fitness jumps. We find that aggregating populations—after meta training—from 10 different experiments is a good way of countering such stochasticity.

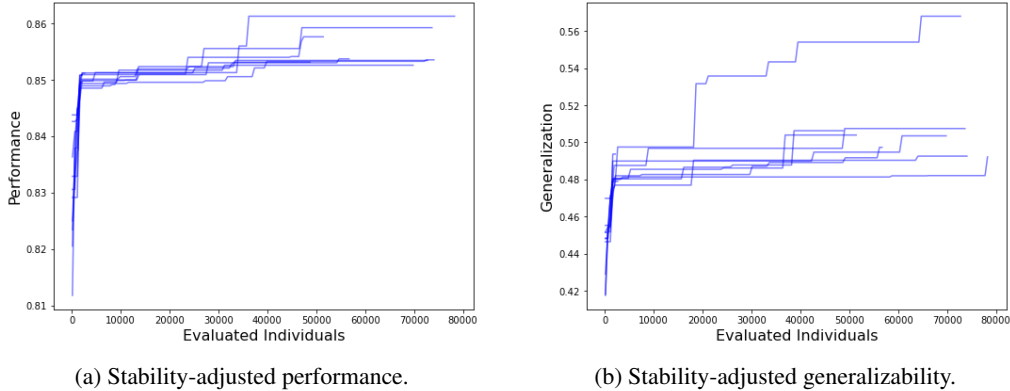


Figure 5: Evolution curves of the best fitness in the population with respect to the total number of evaluated individuals. Figures show 10 identical runs of the evolution experiment using RWRL Cartpole.

C Environment Configurations

In this work we use multiple environments for our experiments: Cartpole and Walker from the RWRL Environment Suite [4], Gym Pendulum, and Ant and Humanoid from the Brax physics simulator [23]. In Table 2 we list the training configuration used for each and the parameters that we use to assess the generalizability of the policies. The parameters that are not listed are fixed to the default values for the environment in question.

In the case of Gym Pendulum and the Brax environments, we have more than one perturbation parameter; the generalizability score is computed by first sweeping through the perturbation values for one, taking the average f_{gen_1} , repeating the same process for the others to compute $f_{gen_2}, \dots, f_{gen_P}$, and then computing the average of both to get the final score, i.e., $f_{gen} = (f_{gen_1} + \dots + f_{gen_P})/P$, where P is the total number of different parameters that are perturbed.

For the parameters that undergo perturbations, we select the specific value used in the training configuration based on the following criteria: in the case of the RWRL Environment Suite, we pick

the training value used in [4], which corresponds to the default value as described in each benchmark; in the case of Gym Pendulum, we pick the default values given by the environment as training configuration; in the case of Brax, we follow the rationale of selecting training configurations that represent a baseline scenario (i.e., no mass variations, normal friction, and normal torque).

Table 2: Environment parameters and perturbations.

Environment parameter	Value
RWRL Cartpole	
Rollout length	1,000
Min. return	0
Max. return	1,000
Training episodes	150
Perturbation parameter (PP)	Pole length
PP Default value	1.0
PP Generalizability values	0.1 to 3.0 in steps of 0.1
RWRL Walker	
Rollout length	1,000
Min. return	0
Max. return	1,000
Training episodes	225
Perturbation parameter (PP)	Thigh length
PP Default value	0.225
PP Generalizability values	.1, .125, .15, .175, .2, .225, .25, .3, .35, .4, .45, .5, .55, .6, .7
Gym Pendulum	
Rollout length	2,000
Min. return	-2,000
Max. return	0
Training episodes	100
Perturbation parameter 1 (PP1)	Pendulum mass
PP1 Default value	1.0
PP1 Generalizability values	.1, .2, .4, .5, .75, 1.0, 1.5, 2.0, 3.0, 5.0, 7.5, 10.0
Perturbation parameter 2 (PP2)	Pendulum length
PP2 Default value	1.0
PP2 Generalizability values	.1, .2, .4, .5, .75, 1.0, 1.5, 2.0, 3.0, 5.0, 7.5, 10.0
Brax environments	
Rollout length	1,000
Min. return	0
Max. return	10,000 (Ant) and 14,000 (Humanoid)
Training episodes	1,000
Perturbation parameter 1 (PP1)	Mass coefficient
PP1 Default value	1.0
PP1 Generalizability values	0.8 to 1.2 in steps of 0.05
Perturbation parameter 2 (PP2)	Friction coefficient
PP2 Default value	1.0
PP2 Generalizability values	0.3 to 1.0 in steps of 0.05
Perturbation parameter 3 (PP3)	Torque multiplier
PP3 Default value	1.0
PP3 Generalizability values	0.5 to 1.0 in steps of 0.05
Perturbation parameter 4 (PP4)	Combined parameters PP1, PP2, and PP3
PP4 Default value	1.0 for each
PP4 Generalizability values	Grid search over individual generalizability values

D warm-start SAC

We present the version of Soft Actor-Critic (SAC) [24] used in this work as the warm-start algorithm to initialize the population. We first present the equations for the policy loss L_{π}^{WS} and critic loss $L_{Q_i}^{WS}$:

$$L_{\pi}^{WS} = \mathbb{E}_{(s_t, a_t) \sim \mathcal{D}} \left[\log \pi(\tilde{a}_t | s_t) - \min_i Q_i(s_t, \tilde{a}_t) \right] \quad (9)$$

$$L_{Q_i}^{WS} = \mathbb{E}_{(s_t, a_t, r_t, s_{t+1}) \sim \mathcal{D}} \left[\left(r_t + \gamma \left(\min_i Q_{targ_i}(s_{t+1}, \tilde{a}_{t+1}) - \log \pi(\tilde{a}_{t+1} | s_{t+1}) \right) - Q_i(s_t, a_t) \right)^2 \right] \quad (10)$$

where $\tilde{a}_t \sim \pi(\cdot | s_t)$, $\tilde{a}_{t+1} \sim \pi(\cdot | s_{t+1})$, and \mathcal{D} is a dataset from the replay buffer. Then, in Figure 6 we represent these two equations that define the SAC algorithm in the form of a graph with typed input and outputs. MetaPG then modifies this graphs following the procedure described in Section 3.

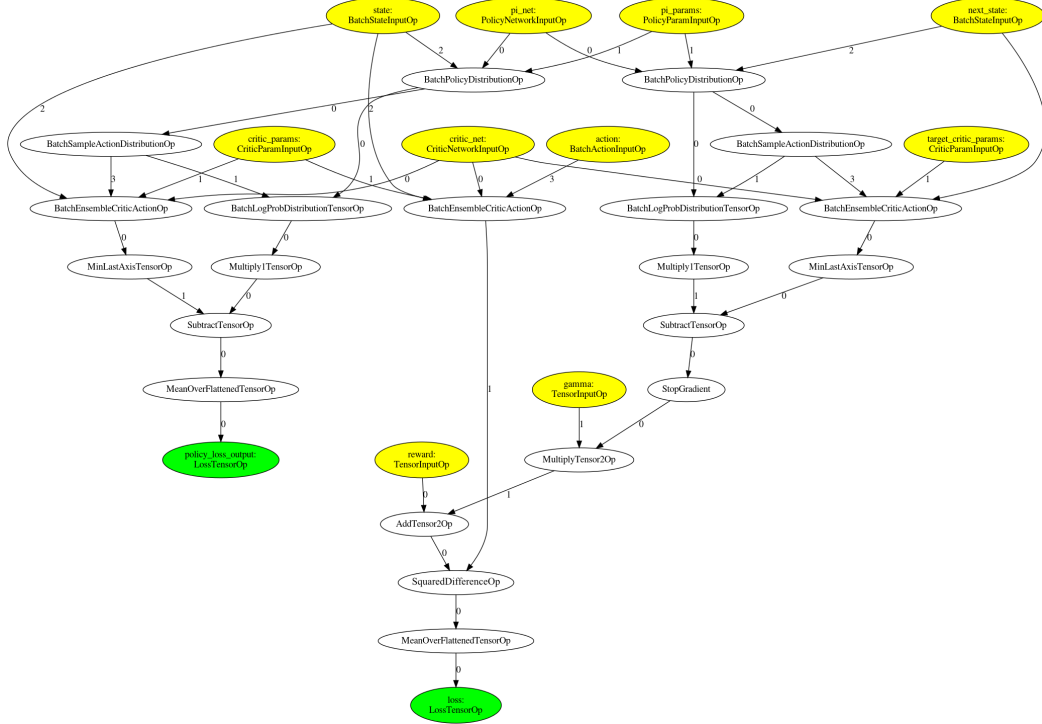


Figure 6: Soft Actor-Critic (SAC) algorithm represented as a graph to initialize the population as a warm-start algorithm.

E Additional RL training details

An individual encoding a RL algorithm in the form of a graph is evaluated by training an agent using such algorithm. We use an implementation based on an ACME agent [55] for the RWRL and Gym environments, and an implementation based on the Brax physics simulator [23] for the Brax environments. The configuration of the training setup are shown in Table 3 for RWRL and Gym environments, and in Table 4 for the Brax environments.

F Additional results

In this section we present the additional results of the paper. We first introduce the remaining figures for RWRL Cartpole, then outline evolution results for RWRL Walker and Gym Pendulum, then show how different algorithms in the population for all three environments compare in terms of stability, then provide results for the Brax environments, then provide the equations of the evolved algorithms, and finally provide more details on other metrics of evolved algorithms.

Table 3: RL Training setup for the RWRL and Gym environments.

Parameter	Value
Discount factor γ	0.99
Batch size	64 (RWRL Cartpole and Gym Pendulum) 128 (RWRL Walker)
Learning rate	$3 \cdot 10^{-4}$
Target smoothing coeff. τ	0.005
Replay buffer size	1,000,000
Min. num. samples in the buffer	10,000
Gradient updates per learning step	1
n step	1
Reward scale	5.0
Actor network	MLP (256, 256)
Actor activation function	ReLU
Tanh on output of actor network	Yes
Critic networks	MLP (256, 256)
Critic activation function	ReLU

Table 4: RL Training setup for the Brax environments.

Parameter	Value
Discount factor γ	0.95
Batch size	128
Learning rate	$6 \cdot 10^{-4}$
Target smoothing coeff. τ	0.005
Replay buffer size	1,000,000
Min. num. samples in the buffer	1,000
Gradient updates per learning step	64
Reward scale	10.0
Number of parallel environments	128
Actor network	MLP (256, 256)
Actor activation function	ReLU
Tanh on output of actor network	Yes
Critic networks	MLP (256, 256)
Critic activation function	ReLU

F.1 Evolution results for RWRL Cartpole

Figure 7 shows the resulting population when running evolution using the RWRL Cartpole environment [4] and Table 5 shows the average fitness scores (\pm standard error of the mean) for each algorithm in the Pareto-optimal set. Figure 8 shows the performance of the evolved algorithms across different environment configurations, it updates Figure 2b by introducing PPO [57] in the comparison. We found that PPO was not well-suited for the continuous control tasks explored in this work.

F.2 Evolution results for RWRL Walker

We present evolution results when running MetaPG with RWRL Walker as the training environment. In Figures 9 and 10 we show the resulting population and the performance across environment configurations for the best performer and the best generalizer in the Pareto-optimal set, respectively. Exact numbers for each algorithm in the Pareto-optimal set can be found in Table 6. This table also shows the scores of the warm-start and ACME SAC. As covered in Appendix F.10, we do not hyperparameter-tune the warm-start before the experiments. As a result, the warm-start might perform poorly, as is the case in this environment. We can observe MetaPG is able to increase the fitness of the evolved algorithms during the evolution process.

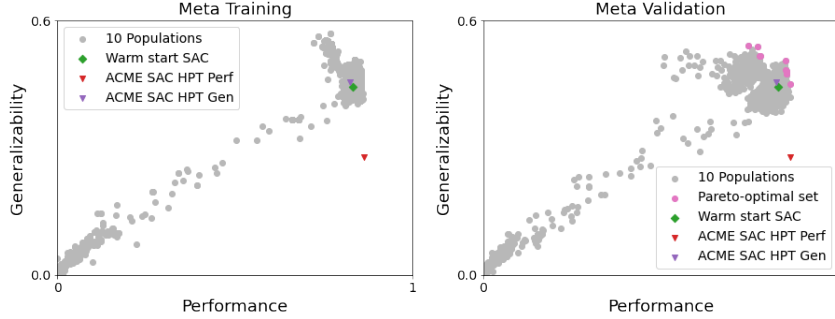


Figure 7: Meta training and meta validation stability-adjusted fitness scores (computed using Equation 3 across 10 seeds) for each RL algorithm in the population alongside the warm-start (SAC) and ACME SAC when using the RWRL Cartpole environment for training. We show the meta validated Pareto-optimal set of algorithms that results after merging the 10 populations corresponding to the 10 repeats of the experiment.

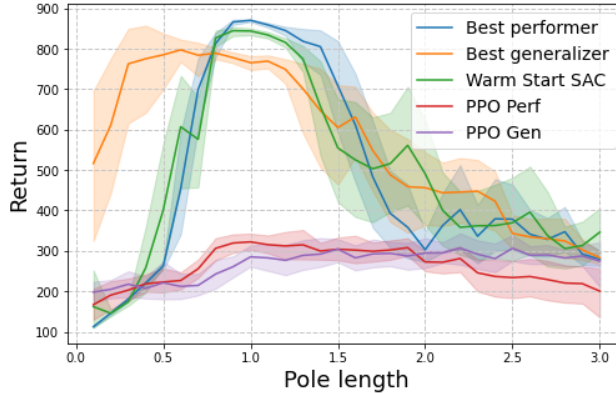


Figure 8: Average and standard deviation across seeds of the meta validation performance when training on a single configuration of RWRL Cartpole and evaluating on multiple unseen ones. We compare the best performer, the best generalizer, the warm start SAC, and we also add two hyperparameter-tuned PPO runs, one tuned for performance and the other for generalizability (see Appendix F.10 for hyperparameter tuning details). The pole length changes across environment configurations and a length of 1.0 is used as training configuration.

F.3 Evolution results for Gym Pendulum

We present evolution results when running MetaPG with Gym Pendulum as the training environment. In Figures 11 and 12 we show the resulting population and the performance across environment configurations for the best performer and the best generalizer in the Pareto-optimal set, respectively. In the case of Pendulum, the generalizability fitness score is computed across the perturbation of two different parameters: the pendulum mass and the pendulum length. These parameters are changed separately, as opposed to varying both the mass and length of the pendulum in the same run. Exact numbers can be found in Table 7, in which an average improvement over the warm-start of 1% in performance and 16% in generalizability is achieved.

F.4 Stability analyses for RWRL Cartpole, RWRL Walker, and Gym Pendulum

We present the stability results, which are accounted for by penalizing the standard deviation across seeds, following Equation 3. For each environment considered in this work, we select a subset of the meta validated graphs that covers all the explored fitness space and, in Figure 13, show the average and standard deviation of each fitness score. Algorithms in the Pareto-optimal set and those closer

Table 5: Average meta-validated performance and generalizability scores (Equations 1 and 2, respectively) \pm standard error of the mean for the 10 algorithms in the Pareto-optimal set and SAC when using RWRL Cartpole as a training environment. We compute these metrics across 10 seeds.

RL Algorithm	Avg. Perf. score (f_{perf})	Avg. Gen. score (f_{gen})
Pareto 1: Best performer	0.871 ± 0.003	0.475 ± 0.016
Pareto 2	0.857 ± 0.001	0.513 ± 0.025
Pareto 3	0.857 ± 0.002	0.514 ± 0.025
Pareto 4	0.856 ± 0.002	0.517 ± 0.024
Pareto 5	0.855 ± 0.002	0.520 ± 0.023
Pareto 6	0.854 ± 0.002	0.531 ± 0.017
Pareto 7	0.798 ± 0.010	0.540 ± 0.016
Pareto 8	0.794 ± 0.010	0.546 ± 0.018
Pareto 9	0.783 ± 0.007	0.579 ± 0.026
Pareto 10: Best generalizer	0.770 ± 0.014	0.570 ± 0.019
warm-start SAC	0.845 ± 0.009	0.487 ± 0.027
ACME SAC HPT Perf	0.865 ± 0.001	0.372 ± 0.060
ACME SAC HPT Gen	0.845 ± 0.012	0.518 ± 0.040

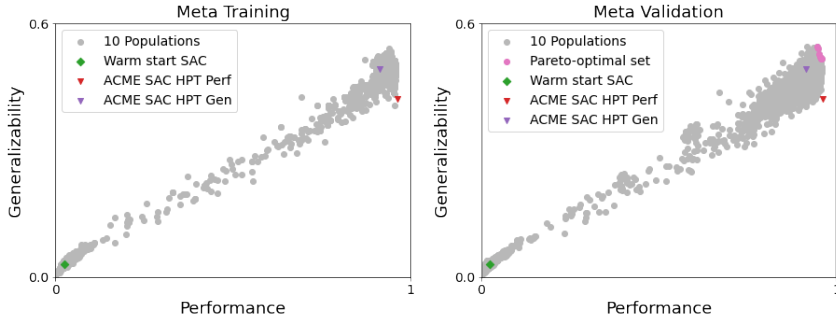


Figure 9: Meta training and meta validation stability-adjusted fitness scores (computed using Equation 3 across 10 seeds) for each RL algorithm in the population alongside the warm-start (SAC) and ACME SAC when using the RWRL Walker environment for training. We show the meta validated Pareto-optimal set of algorithms that results after merging the 10 populations corresponding to the 10 repeats of the experiment.

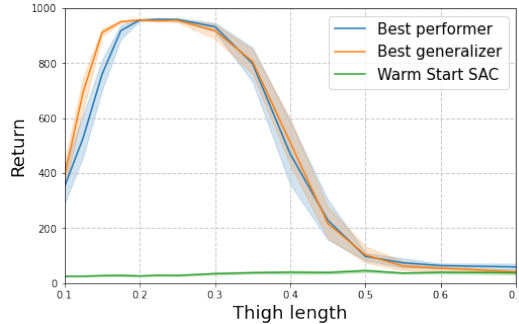


Figure 10: Average and standard deviation across seeds of the meta validation performance of the best performer, the best generalizer, and the warm-start (SAC) when training on a single configuration of RWRL Walker and evaluating on multiple unseen ones. The thigh length changes across environment configurations and a length of 0.225 is used as training configuration.

to it present lower variability, showing MetaPG is also successful in improving the stability of RL algorithms.

Table 6: Average meta-validated performance and generalizability scores (Equations 1 and 2, respectively) \pm standard error of the mean for the 7 algorithms in the Pareto-optimal set and SAC when using RWRL Walker as a training environment. We compute these metrics across 10 seeds.

RL Algorithm	Avg. Perf. score (f_{perf})	Avg. Gen. score (f_{gen})
Pareto 1: Best performer	0.963 ± 0.002	0.544 ± 0.018
Pareto 2	0.962 ± 0.003	0.536 ± 0.012
Pareto 3	0.960 ± 0.002	0.542 ± 0.015
Pareto 4	0.959 ± 0.003	0.541 ± 0.013
Pareto 5	0.960 ± 0.005	0.541 ± 0.009
Pareto 6	0.954 ± 0.003	0.555 ± 0.009
Pareto 7: Best generalizer	0.955 ± 0.005	0.569 ± 0.015
warm-start SAC	0.028 ± 0.002	0.033 ± 0.001
ACME SAC HPT Perf	0.968 ± 0.003	0.444 ± 0.014
ACME SAC HPT Gen	0.926 ± 0.008	0.510 ± 0.012

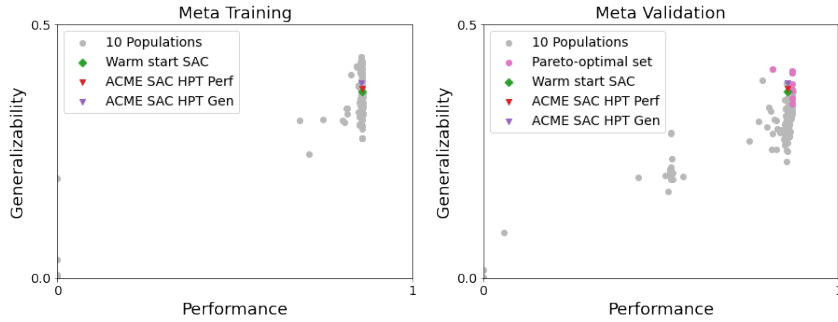


Figure 11: Meta training and meta validation stability-adjusted fitness scores (computed using Equation 3 across 10 seeds) for each RL algorithm in the population alongside the warm-start (SAC) and ACME SAC when using the Gym Pendulum environment for training. We show the meta validated Pareto-optimal set of algorithms that results after merging the 10 populations corresponding to the 10 repeats of the experiment.

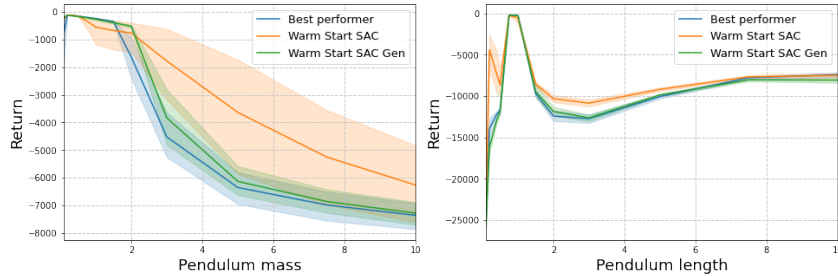


Figure 12: Average and standard deviation across seeds of the meta validation performance of the best performer, the best generalizer, and the warm-start (SAC) when training on a single configuration of Gym Pendulum and evaluating on multiple unseen ones. The pendulum mass and the pendulum length independently change across environment configurations (we change one at a time). The training configurations use a pendulum mass and a pendulum length of 1.0 and 1.0, respectively.

F.5 Evolution results for Brax Ant

Table 8 shows the meta testing fitness scores of the best performer algorithms obtained after running evolution on Brax Ant and Brax Humanoid, respectively. We compare those against the hyperparameter-tuned warm-start SAC and observe an improvement of 12% and 9% in performance and generalizability, respectively, and up to a 24% reduction in instability. We observe that, after

Table 7: Average meta-validated performance and generalizability scores (Equations 1 and 2, respectively) \pm standard error of the mean for the 8 algorithms in the Pareto-optimal set and SAC when using Gym Pendulum as a training environment. We compute these metrics across 10 seeds.

RL Algorithm	Avg. Perf. score (f_{perf})	Avg. Gen. score (f_{gen})
Pareto 1: Best performer	0.887 ± 0.010	0.360 ± 0.011
Pareto 2	0.885 ± 0.009	0.381 ± 0.017
Pareto 3	0.887 ± 0.010	0.391 ± 0.014
Pareto 4	0.887 ± 0.011	0.392 ± 0.013
Pareto 5	0.887 ± 0.011	0.393 ± 0.007
Pareto 6	0.886 ± 0.010	0.433 ± 0.018
Pareto 7	0.886 ± 0.011	0.437 ± 0.019
Pareto 8: Best generalizer	0.868 ± 0.034	0.445 ± 0.021
warm-start SAC	0.879 ± 0.022	0.383 ± 0.015
ACME SAC HPT Perf	0.880 ± 0.014	0.392 ± 0.012
ACME SAC HPT Gen	0.879 ± 0.014	0.400 ± 0.009

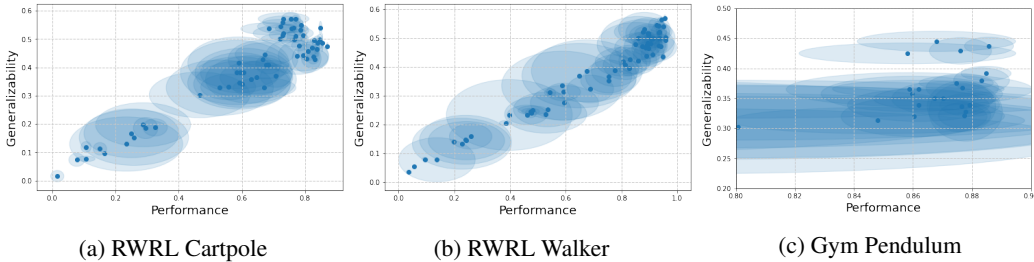


Figure 13: From a subset of the meta validated graphs, for each of them, we show the average fitness scores surrounded by an ellipse with semiaxes representing the standard deviation across seeds for each fitness score.

cross-domain transfer, the algorithm evolved in Brax Humanoid achieves comparable scores to SAC. We follow the hyperparameter tuning procedure explained in Appendix F.11.

Table 8: Average meta-tested performance and generalizability scores (Equations 1 and 2, respectively) \pm standard error of the mean for algorithms first evolved in Brax Ant and Brax Humanoid, and then evaluated on Brax Ant on a different set of seeds. We compare these scores against the hyperparameter-tuned warm start SAC. We compute these metrics across 4 seeds.

RL Algorithm	Avg. Perf. score (f_{perf})	Avg. Gen. score (f_{gen})
Ant performer	0.770 ± 0.041	0.627 ± 0.035
Humanoid performer	0.643 ± 0.117	0.553 ± 0.086
warm-start SAC	0.685 ± 0.053	0.573 ± 0.036

F.6 Evolution results for Brax Humanoid

Figure 14 shows the behaviour of evolved algorithms when meta-tested in Brax Humanoid, using an evaluation consisting of perturbations encountered in many practical settings (changes in friction coefficient, mass, and torque), as outlined in Appendix C. We first evolve algorithms independently in both Humanoid and Ant, then, for each case, select the algorithm with the best performance \tilde{f}_{perf} (in this case we focus on only one of the evolved algorithms since there is strong correlation between both metrics; the best performer and best generalizer are close, sometimes even encode the same algorithm), then meta-validate it with different hyperparameter sets (see Appendix F.11), and select the hyperparameter set that leads to the best generalizability. We then fix the hyperparameters and re-evaluate using the meta-testing seeds. We compare algorithms evolved in Ant and Humanoid with hyperparameter-tuned SAC.

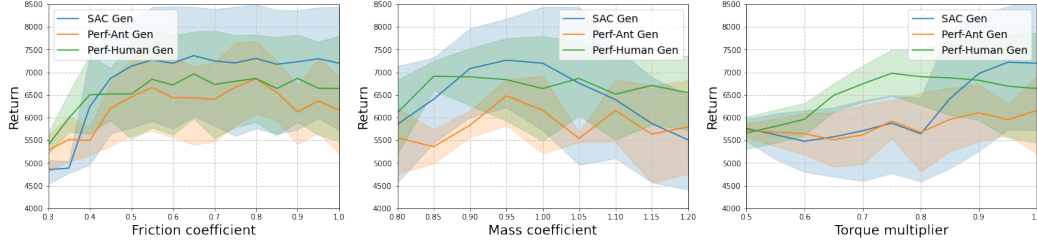


Figure 14: Average return and standard deviation across random seeds when evaluating evolved algorithms and SAC baseline in multiple Brax Humanoid instances with different friction coefficients, mass coefficients, and torque multipliers. We compare, after hyperparameter tuning, algorithms evolved in Brax Humanoid, Brax Ant (to assess cross-domain transfer), and the SAC baseline used as warm-start. In all cases 1.0 is used as training configuration.

The numerical results of this analysis are found in Table 9. We observe that, while the evolved algorithm achieves better generalizability and a clear reduction in instability (up to 40%), the evolved algorithm performs worse than SAC when meta testing. In this case the algorithms are hyperparameter-tuned for generalizability, hence the higher score. Note we evolved less graphs in the specific case of Humanoid (50K compared to 200K evolved graphs for Brax Ant), as training a policy in Humanoid is more costly. We expect these results to improve if more algorithms are evolved in the population. Then, as in the case where we used Brax Ant as evaluation environment, we achieve a good cross-domain fitness compared to SAC, but the scores are lower. In this case, however, the algorithm evolved in Brax Ant shows more stability than SAC when both are evaluated in Humanoid.

Table 9: Average meta-tested performance and generalizability scores (Equations 1 and 2, respectively) \pm standard error of the mean for algorithms first evolved in Brax Ant and Brax Humanoid, and then evaluated on Brax Humanoid on a different set of seeds. We compare these scores against the hyperparameter-tuned warm start SAC. We compute these metrics across 4 seeds.

RL Algorithm	Avg. Perf. score (f_{perf})	Avg. Gen. score (f_{gen})
Ant performer	0.440 ± 0.066	0.420 ± 0.036
Humanoid performer	0.474 ± 0.083	0.462 ± 0.042
warm-start SAC	0.514 ± 0.104	0.450 ± 0.070

F.7 Best performer and best generalizer for RWRL Walker and Gym Pendulum

We present the loss equations for both the best performer and best generalizer when using RWRL Walker and Gym Pendulum as training environments. First, the best performer for RWRL Walker:

$$L_{\pi}^{perf} = \mathbb{E}_{(s_t, a_t, r_t, s_{t+1}) \sim \mathcal{D}} \left[r_t + \gamma \left(\min_i Q_{target_i}(s_{t+1}, \tilde{a}_{t+1}) - \text{atan}(\gamma/Q(s_t, a_t)) \right) - Q(s_t, \tilde{a}_t) \right] \quad (11)$$

$$L_{Q_i}^{perf} = \mathbb{E}_{(s_t, a_t, r_t, s_{t+1}) \sim \mathcal{D}} \left[\left(r_t + \gamma \left(\min_i Q_{target_i}(s_{t+1}, \tilde{a}_{t+1}) - \text{atan}(\gamma/Q_i(s_t, a_t)) \right) - Q_i(s_t, a_t) \right)^2 \right] \quad (12)$$

In all cases, $\tilde{a}_t \sim \pi(\cdot|s_t)$, $\tilde{a}_{t+1} \sim \pi(\cdot|s_{t+1})$, and \mathcal{D} is a dataset of experience tuples from the replay buffer. Next, the best generalizer for RWRL Walker:

$$L_{\pi}^{gen} = \mathbb{E}_{(s_t, a_t, s_{t+1}) \sim \mathcal{D}} \left[\frac{0.2 \cdot \log \pi(\tilde{a}_{t+1}|s_{t+1})}{Q_i(s_{t+1}, \tilde{a}_{t+1}) - 0.1 \cdot \log \pi(\tilde{a}_{t+1}|s_{t+1})} - \min_i Q_i(s_t, \tilde{a}_{t+1}) \right] \quad (13)$$

$$L_{Q_i}^{gen} = \mathbb{E}_{(s_t, a_t, r_t, s_{t+1}) \sim \mathcal{D}} \left[\left(r_t + \gamma \left(Q_i(s_{t+1}, \tilde{a}_{t+1}) - 0.1 \cdot \log \pi(\tilde{a}_{t+1}|s_{t+1}) \right) - Q_i(s_t, a_t) \right)^2 \right] \quad (14)$$

Now we present the best performer for Gym Pendulum:

$$L_{\pi}^{perf} = \mathbb{E}_{(s_t, a_t) \sim \mathcal{D}} \left[2 \cdot \text{atan}(\log \pi(\tilde{a}_t | s_t)) - \min_i Q_i(s_t, \tilde{a}_t) \right] \quad (15)$$

$$L_{Q_i}^{perf} = \mathbb{E}_{(s_t, a_t, r_t, s_{t+1}) \sim \mathcal{D}} \left[(r_t + \gamma (Q_{\text{target}_i}(s_{t+1}, \tilde{a}_t) - \log \pi(\tilde{a}_t | s_t)) - Q_i(s_t, a_t))^2 \right] \quad (16)$$

Finally, the equations for the best generalizer when using Gym Pendulum are:

$$L_{\pi}^{gen} = \mathbb{E}_{(s_t, a_t) \sim \mathcal{D}} \left[\log(\log \pi(\tilde{a}_t | s_t)) - \min_i Q_i(s_t, \tilde{a}_t) \right] \quad (17)$$

$$L_{Q_i}^{gen} = \mathbb{E}_{(s_t, a_t, r_t, s_{t+1}) \sim \mathcal{D}} \left[(r_t + \gamma (Q_{\text{target}_i}(s_{t+1}, \tilde{a}_t) - \log(\log \pi(\tilde{a}_t | s_t))) - Q_i(s_t, a_t))^2 \right] \quad (18)$$

F.8 Best performer for Brax Ant and Brax Humanoid

We present the loss equations (policy loss and critic loss) for the best performer algorithms evolved in Brax Ant and Brax Humanoid; we focus on these two algorithms in the analyses of this paper. The loss functions for the best performer for Brax Ant are:

$$L_{\pi}^{perf} = \mathbb{E}_{(s_t, a_t) \sim \mathcal{D}} \left[\log \pi(\tilde{a}_{t+1} | s_{t+1}) - \min_i Q_i(s_t, a_t) \right] \quad (19)$$

$$L_{Q_i}^{perf} = \mathbb{E}_{(s_t, a_t, r_t, s_{t+1}) \sim \mathcal{D}} \left[\left(r + \gamma \left(\min_i Q_{\text{target}_i}(s_t, \tilde{a}_{t+1}) - \gamma \right) - Q_i(s_t, a_t) \right)^2 \cdot C_1 \right] \quad (20)$$

where

$$C_1 = r_t + \gamma \cdot \left(\min_i Q_i(s_{t+1}, \tilde{a}_{t+1}) - \gamma \right) \quad (21)$$

In all cases, $\tilde{a}_{t+1} \sim \pi(\cdot | s_{t+1})$ and \mathcal{D} is a dataset of experience tuples from the replay buffer. Then, the equations for the best performer evolved in Brax Humanoid are:

$$L_{\pi}^{perf} = \mathbb{E}_{(s_t, a_t) \sim \mathcal{D}} \left[\log \pi(\tilde{a}_{t+1} | s_{t+1}) - \min_i Q_i(s_t, a_t) \right] \quad (22)$$

$$L_{Q_i}^{perf} = \mathbb{E}_{(s_t, a_t, r_t, s_{t+1}) \sim \mathcal{D}} \left[(C_2 - Q_i(s_t, a_t))^2 \cdot C_2 \right] \quad (23)$$

where

$$C_2 = r_t + \gamma \left(\min_i Q_{\text{target}_i}(s_t, \tilde{a}_{t+1}) - \log \pi(\tilde{a}_{t+1} | s_{t+1}) \right) \quad (24)$$

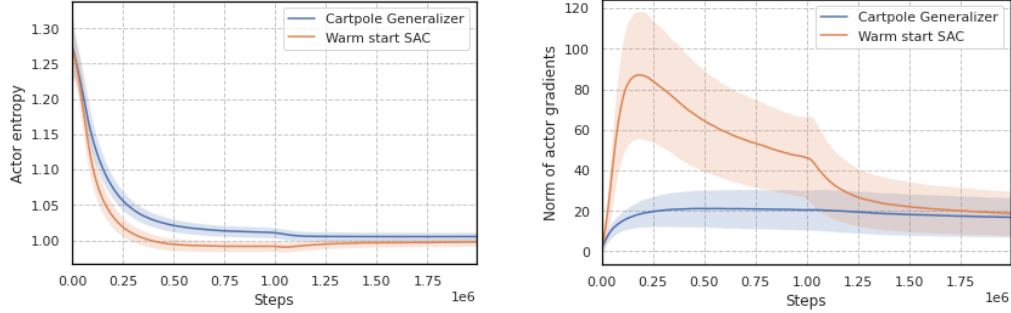
F.9 Additional analysis on evolved algorithms for RWRL Cartpole

Figure 15 shows the entropy and norm of the gradients of the actor for the RWRL Cartpole best generalizer. We also show these same metrics for the warm-start algorithm. This is an extension of Figure 4; in both cases, we let the agents train for more episodes than those in the experimental setup. We see that ignoring this fixed number of training episodes and letting run for longer makes this type of metrics converge to similar values across algorithms. We acknowledge that training until convergence is usually preferred; however, in certain applications the number of training episodes might be a constraint, so we find MetaPG’s ability to exploit this kind of constraints beneficial in those setups.

F.10 Hyperparameter tuning for transfer and benchmark for RWRL and Gym

In our experiments with the RWRL Environment suite and Gym Pendulum, once an evolution experiment is over and the evolved algorithms are meta-validated, we compare them against: 1) ACME SAC [55], and 2) other RL algorithms that have been evolved in a different environment. To that end, for each ACME benchmark and evolved algorithm transfer, we tune the hyperparameters of the algorithms. Since we consider two fitness scores in this work (performance and generalizability), we select the two hyperparameter configurations that lead to the best performance and best generalizability scores, respectively. We denote these two configurations as the best performer and best generalizer, respectively. To that end, we do a grid search across the sets of hyperparameters listed in Table 10.

This process is only carried out once the evolution is over; the warm-start algorithm is not hyperparameter-tuned before evolution.



(a) Average entropy of the policy during training for RWRL Cartpole. (b) Average gradient norm of the actor loss during training for RWRL Cartpole.

Figure 15: Analysis of the entropy and gradient norm of the actor when evaluating the best generalizer from RWRL Cartpole in comparison to the warm-start.

Table 10: Hyperparameter values considered during the tuning process.

Hyperparameter	Values
Discount factor γ	0.9, 0.99, 0.999
Batch size	32, 64, 128
Learning rate	$1 \cdot 10^{-4}$, $3 \cdot 10^{-4}$, $1 \cdot 10^{-3}$
Target smoothing coeff. τ	0.005, 0.01, 0.05
Reward scale	0.1, 1.0, 5.0, 10.0

F.11 Hyperparameter tuning for transfer and benchmark for Brax

In our experiments in Brax Ant and Brax Humanoid, given they are more costly environments, we do not meta validate all algorithms in the population. Instead, we choose the best algorithms during meta training and directly meta test them with additional hyperparameter tuning. To that end, we do a grid search across the hyperparameters listed in Table 11 and select the configuration that maximizes the score we are interested in for each case, as described in the previous section.

Table 11: Hyperparameter values considered during the tuning process.

Hyperparameter	Values
Discount factor γ	0.95, 0.99, 0.999
Batch size	128, 256, 512
Learning rate	$1 \cdot 10^{-4}$, $6 \cdot 10^{-4}$, $1 \cdot 10^{-3}$
Gradient updates per learning step	32, 64, 128
Reward scale	0.1, 1.0, 10.0, 100.0

F.12 Transferring algorithms evolved in RWRL and Gym

We present the results of carrying out transfer experiments in which we take the best performer and best generalizer obtained after evolving in a specific environment and test them in the other two environments considered in this work. To that end, we follow the hyperparameter tuning procedure described above and therefore, for each different RL algorithm, we obtain the hyperparameter configurations that leads to the best performance and best generalizability, respectively. For example, taking the best performer from RWRL Walker (Walker Perf.) and testing it on RWRL Cartpole leads to two sets of fitness scores (best performer and best generalizer). The transfer results for RWRL Cartpole, RWRL Walker, and Gym Pendulum can be observed in Tables 12, 13, and 14, respectively.

Table 12: Transfer results (average fitness \pm standard error of the mean) on RWRL Cartpole. The row highlighted in gray corresponds to the results of the evolution experiment in RWRL Cartpole. The rest correspond to the best performance and best generalizability configurations that result from doing hyperparameter tuning to the best performer and best generalizer evolved in different environments.

Evaluation and tuning environment: RWRL Cartpole				
RL Algorithm	Best performance		Best generalizability	
	f_{perf}	f_{gen}	f_{perf}	f_{gen}
Cartpole	0.871 \pm 0.003	0.475 \pm 0.016	0.770 \pm 0.014	0.570 \pm 0.019
Walker Perf.	0.849 \pm 0.010	0.444 \pm 0.041	0.826 \pm 0.024	0.456 \pm 0.041
Walker Gen.	0.670 \pm 0.094	0.374 \pm 0.039	0.670 \pm 0.094	0.374 \pm 0.039
Pendulum Perf.	0.857 \pm 0.001	0.502 \pm 0.024	0.851 \pm 0.005	0.535 \pm 0.012
Pendulum Gen.	0.829 \pm 0.025	0.489 \pm 0.051	0.766 \pm 0.079	0.509 \pm 0.040
ACME SAC	0.865 \pm 0.001	0.372 \pm 0.060	0.845 \pm 0.012	0.518 \pm 0.040

Table 13: Transfer results (average fitness \pm standard error of the mean) on RWRL Walker. The row highlighted in gray corresponds to the results of the evolution experiment in RWRL Walker. The rest correspond to the best performance and best generalizability configurations that result from doing hyperparameter tuning to the best performer and best generalizer evolved in different environments.

Evaluation and tuning environment: RWRL Walker				
RL Algorithm	Best performance		Best generalizability	
	f_{perf}	f_{gen}	f_{perf}	f_{gen}
Cartpole Perf.	0.959 \pm 0.004	0.502 \pm 0.025	0.958 \pm 0.006	0.533 \pm 0.012
Cartpole Gen.	0.031 \pm 0.002	0.032 \pm 0.001	0.027 \pm 0.003	0.035 \pm 0.001
Walker	0.963 \pm 0.002	0.544 \pm 0.018	0.955 \pm 0.005	0.569 \pm 0.015
Pendulum Perf.	0.611 \pm 0.145	0.296 \pm 0.066	0.611 \pm 0.145	0.296 \pm 0.066
Pendulum Gen.	0.929 \pm 0.024	0.510 \pm 0.045	0.927 \pm 0.024	0.518 \pm 0.035
ACME SAC	0.968 \pm 0.003	0.444 \pm 0.014	0.926 \pm 0.008	0.510 \pm 0.012

Table 14: Transfer results (average fitness \pm standard error of the mean) on Gym Pendulum. The row highlighted in gray corresponds to the results of the evolution experiment in Gym Pendulum. The rest correspond to the best performance and best generalizability configurations that result from doing hyperparameter tuning to the best performer and best generalizer evolved in different environments.

Evaluation and tuning environment: Gym Pendulum				
RL Algorithm	Best performance		Best generalizability	
	f_{perf}	f_{gen}	f_{perf}	f_{gen}
Cartpole Perf.	0.875 \pm 0.013	0.352 \pm 0.023	0.874 \pm 0.017	0.364 \pm 0.015
Cartpole Gen.	0.843 \pm 0.022	0.337 \pm 0.014	0.843 \pm 0.022	0.337 \pm 0.014
Walker Perf.	0.873 \pm 0.013	0.342 \pm 0.018	0.843 \pm 0.030	0.395 \pm 0.020
Walker Gen.	0.864 \pm 0.015	0.349 \pm 0.030	0.754 \pm 0.075	0.401 \pm 0.013
Pendulum	0.887 \pm 0.010	0.360 \pm 0.011	0.868 \pm 0.034	0.445 \pm 0.021
ACME SAC	0.879 \pm 0.014	0.392 \pm 0.012	0.879 \pm 0.014	0.400 \pm 0.009